Chemical Engineering Journal 315 (2017) 67–82

Contents lists available at ScienceDirect

Chemical Engineering Journal

journal homepage: www.elsevier.com/locate/cej

Design and characterization of a stagnation flow reactor for heterogeneous microkinetic studies

F. Zanier, N. Michelon, P. Canu *

Industrial Engineering Department, University of Padua, Via Marzolo, 9, 35131 Padua, Italy

HIGHLIGHTS

- Alternative reactor to integrate Surface Science and Industrial catalysis.
- Development of a flexible, yet simple reactor for catalytic film testing.
- Detailed simulation reveals conditions for transport limitation interferences.
- Heat transport in the gas phase is more critical than diffusion limitations.
- Unexpected predictions on dominant role of heat transfer confirmed by experiments.

ARTICLE INFO

Article history:
Received 16 August 2016
Received in revised form 8 January 2017
Accepted 9 January 2017
Available online 10 January 2017

Keywords:
Reactive films
Stagnation-point flow
Pressure gap
Kinetic studies
Pt
H_2 oxidation

ABSTRACT

By modelling of mass, momentum and thermal energy transport we critically investigated the design of a flexible testing cell. Its purpose is carrying out reactivity tests at high pressure ($\geqslant$1 bar) on flat, disk-shaped active surfaces, under continuous gas flow. We revisited the stagnation-point flow arrangement to quantitatively evaluate the potential and the critical factors affecting the experimental information achievable. We investigated the constructive and the operating parameters. Specifically, geometry, contact time, temperature, rate of surface reaction, reactant diffusivity, carrier thermal conductivity, and heat of reaction were parametrically varied. Simulations confirm that reactions can become limited by reactant diffusion at high temperature (i.e. fast reactions), in a perfectly isothermal cell. However, the heat of reactions can easily distort the surface temperature distribution, as evidenced by 2D simulations; thus, the flow structure in the testing cell and the carrier heat conduction become the controlling factors, determining the reaction extent. Finally, a prototype was built and operated using H_2 oxidation on a polycrystalline Pt disk, as probe catalyst and reaction. Measurements confirm the consistency of the simulation study, revealing the critical role played by the unexpected local temperature distribution on the active surface, largely prevailing on any mass diffusion limitation in determining the apparent activity of the surface.

1. Introduction

Progress in the understanding of catalytic mechanisms takes place through measurements on either well defined and ordered surfaces, or on powders. In the first case, surfaces are single crystals cut along low Miller index planes or more complex structures build upon them [1]. Model surfaces are expected to provide fundamental understanding on the surface chemistry, supporting the design of actual catalysts for industrial applications. Powders in contrast are characterized by low coordinated sites (steps, kinks, vacancies and other defects), that can dramatically change the surface mechanism, as suggested by several structure-reactivity studies [2]. The different activity of ideal surfaces vs. powders is sometimes referred as the structure gap [3]. It justifies some divergence of methods and practical conclusions that do not support an effective transfer of knowledge from the scientific to the industrial communities.

Structure gap can be partially overcome using single crystal surfaces cut along high Miller index planes [3,4]; having steps and kinks, they approximate the defective industrial catalyst surfaces. Unfortunately, only one type of defect at a time can be studied by this technique. Other Surface Science techniques allow the growth and self-assembling of thin films on nanostructured templating surfaces [5,6], aimed at controlling the active sites atomic structure, approaching the complexity of industrial catalysts.

* Corresponding author.
E-mail address: paolo.canu@unipd.it (P. Canu).

http://dx.doi.org/10.1016/j.cej.2017.01.028
1385-8947/

In addition, the investigation on model surfaces is carried out in ultra-high vacuum (UHV) [5,7,8], determining a pressure gas. Attempts to overcome it are limited by the pressure allowed by the measurement instruments, so that 'near ambient' versions were developed. Still, the high pressure claimed is just relatively high, with respect to UHV, but in practice well below 1 bar, in the tenths of mbar range [10], as required to use low energy electron and ion-based experimental techniques without undue interference from gas phase scattering.

The model surfaces are almost exclusively prepared as samples that are macroscopically flat, not powders [11]. The samples can be from mm to cm in size; often it is a surface film that brings the chemically specific activity. The reactivity of model surfaces is determined with appropriate testing devices, typically UHV chambers, possibly with static atmosphere, by carrying out local measurements of surface events [1,12]. We may call the limitation in the testing devices the reactor gap. To further support the indication of Surface Science techniques and link them to actual, macroscopic activity, a significant step would be the possibility of testing the global reactivity of such model surface samples. Global, or integral reactivity of an active surface is meant to be the result of the catalytic function over the whole surface, as opposed to local measurements. Global reactivity measurement requires appropriate testing devices (i.e. reactors) operating on model surfaces at higher pressure ($\geqslant$1 bar), higher concentration of reactants and possibly under flow conditions. We believe that the overall reactants conversion and selectivity given by a model surfaces, at industrially relevant conditions, is a macroscale confirmation of the microkinetic models. Macroscale behavior of model surfaces must prove whether the surface mechanisms actually determine a meaningful, complete catalytic path for the reaction under study, rather than just a few, local steps in the mechanism, possibly changing within a complete reaction mechanism. In addition, a consolidated concept of catalyst as a species with invariant properties that can facilitate reactions, but it is not affected by the environment is being questioned by modern approaches and evidences [9,13]. That urges the investigation of the surface reactivity in a representative, not idealized, environment. Measuring the global reactivity of model surfaces is also expected to contribute to the development and validation of microkinetic models of surface reactions, profitably complementing the detailed information of DFT calculations [13–16]. Macroscopic testing of pure metal surfaces in flow reactors has been done in the past, mostly confined to noble metals foils [17–19] or wires [20,21], typically without a precise control of the surface crystal structure. While simple in principle, the quantitative analysis of such experiments may yield unexpected results [22]. We believe that the detailed characterization of the testing device is a perquisite to extract meaningful information from model surfaces.

Here we present a systematic numerical analysis of the stagnation flow configuration, which is a general flow arrangement that nicely fits the testing of disk-shaped, flat model surfaces for global activity. Its modelling [23,24] has been developed into standard applications [25,26] under some simplifying assumptions discussed below, aimed at developing and validating microkinetic models. Still, contradictory experimental results that we obtained suggest that a thorough understanding of its operation and critical features requires additional investigation. We used a model reaction to numerically assess the possible role of heat and mass transfer limitations at isothermal or adiabatic operation, as discussed also by Others [27]. Through parametric studies, we designed a versatile testing cell, for any disk-shaped reacting surface.

The experimental validation on H_2 oxidation on Pt as model reaction proves that mass diffusion is not the controlling process. The temperature spatial distribution turned out to be the key determining factor, severely distorting the apparent activity measurements. We believe that these results can explain previous discrepancies in the Literature, where the light-off temperature of H_2-air mixtures differ by more than 50 K.

2. The stagnation point flow (SPF)

A heterogeneous fluid-solid reaction based on a disk-shaped, planar surface can be effectively carried out under stagnation flow, as shown in Fig. 1. The arrangement has been used since a long time for thin, epitaxial film growth, to be used in electronic and optoelectronic applications [28]. It has been also suggested and widely used for catalytic studies [17,24,31]. In its original design, the disk is often rotating, and the gas is fed in the chamber well above the surface, at a distance that can be several disk diameters [28]. The deposition of epilayers was found to be affected by the gas dynamics on front of the surface, because of mass transfer limitations. Experimental [28,29] and computational studies [29,30] have been carried out to visualize, identify and predict the regimes that develops in front of the solid surface. Gas has been fed by a centered jet (a very common industrial configuration), swirling jets, and porous layers. Stable and unstable regimes have been observed, and three reference flow arrangements (rotational, buoyant, and plug) identified. Flow maps have been developed to predict the prevailing regime, based on Grashof and Reynolds numbers [29]. The optimal configuration aims at developing a plug flow over the surface, with the minimum boundary layer thickness, to improve mass transfer rates to the surface. It can be obtained by feeding the gas through a porous diffuser, possibly larger that the disk, at fairly short distance for the surface (fractions of disk diameters), at a flow rate large enough to contrast buoyancy-driven recirculations [30]. Such a design aims at an effective and uniform transport of gas reactants to the surface, for its regular growth.

Here we suggest a variation of this arrangement, allowing to measure the activity of a catalytic surface by changes in the gas composition. In addition to an effective, stable and reproducible contact with the surface, most of the gas must reach the surface, to measure appreciable variations in its outlet composition. Accordingly, we focused on the centered arrangement shown in Fig. 1, right, where the inlet mixture is focused at the center of the surface and spreads radially towards the surface periphery. We call such a flow configuration towards a reactive surface a *Stagnation Point Flow Reactor* (SPFR). Guiding the divergence of the flow (see Fig. 2) further allows to keep it parallel to the surface, at sufficiently high velocities to dominate any buoyancy effect and achieving short catalyst contact times. The momentum-dominated, parallel, diverging flow is also expected to be better described by simpler reactive flow models, directly involving surface chemistry, of any complexity.

The stagnation flow configuration using a distributed inlet can be simulated with restrictive assumptions, by a 1D model, using a suitable change of variables [24], [32]. The 1D domain can be extended to include a porous catalytic layer [33]. In this study we focus on model catalyst that are non-porous; only external mass transfer is meaningful. Implementations of the 1D model that allow for detailed surface chemistry are available both in the CHEMKIN [25] and Cantera [26] simulation environments. To account for the actual arrangement of the inflowing stream, without any restrictive assumption, we simulated the SPF with a flexible and widely validated computational fluid dynamics (CFD) codes. We used one *COMSOL Multiphysics*, [34] to investigate the effective role of the inlet size, as well as other design parameters, preliminary to the construction of a test cell. The Comsol simulation code can also be interfaced with Cantera [35], for kinetic studies using detailed surface chemistry. Thus, it becomes a useful tool for activity measurements analysis and interpretation, in addition

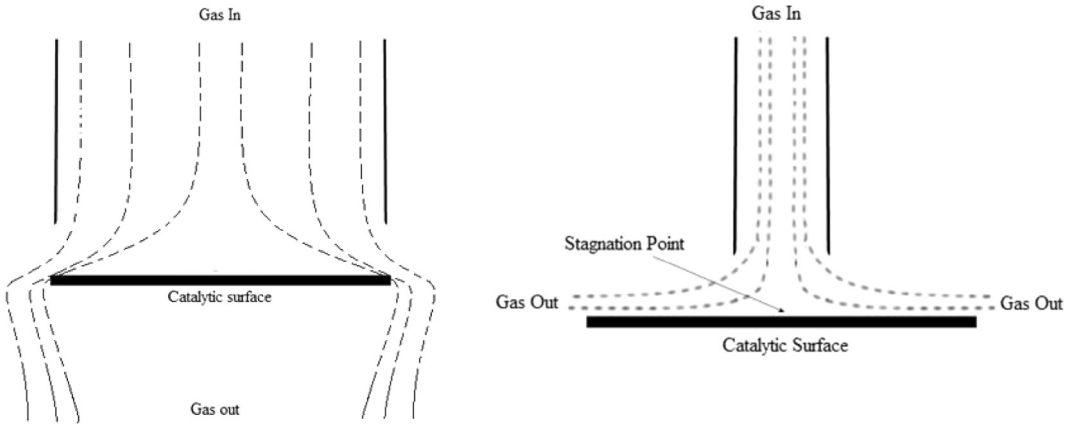

Fig. 1. Stagnation flow (left) and implementation by central jet (right).

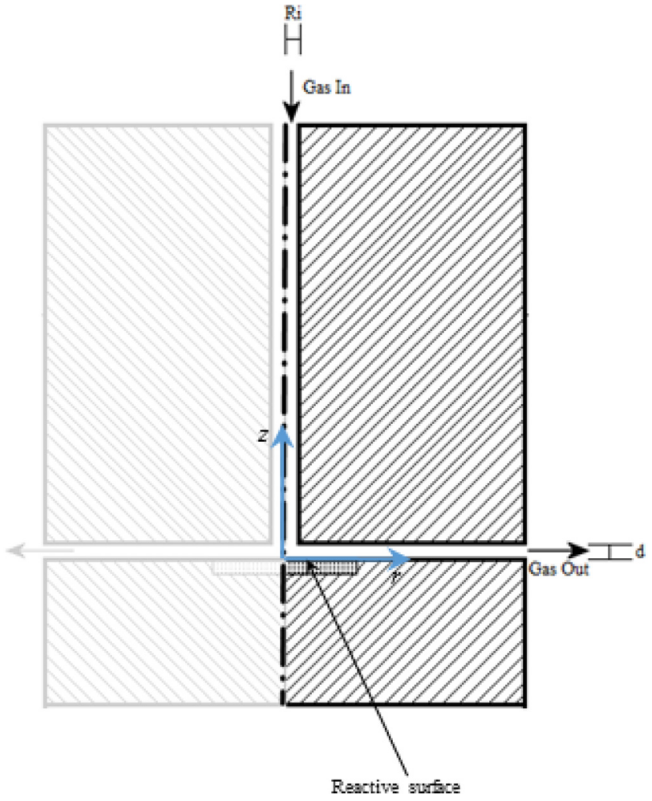

Fig. 2. Model of the stagnation point flow testing cell. Simulation exploits the axial symmetry.

to its support in the design of the test cell. The combination of tools (Comsol and Cantera) used in this work is by no means the unique option to couple gas-phase transport and hetereogeneous reactions, that could possibly be very detailed. Commercial solutions are available by ANSYS, coupling FLUENT with the CHEMKIN tools, and research codes, such as CatalyticFoam [36] and DETCHEM [37,33].

3. A model of reactive, stagnation point flow

The SPFR concept shown in Fig. 1, left, has been implemented in a realistic geometry, as shown in Fig. 2 that schematically reproduces the gas phase domain within the solid boundaries. We take advantage of the axial symmetry; Fig. 2 highlights a semi-section of the SPFR, the actual computation domain. The geometry is parametric, to easily modify the most relevant lengths. These include the radius of the central inlet pipe, R_i, the gap between the bottom surface, which includes the catalytic surface, and its ceiling, d, constraining the radial flow, and the disk radius. These are the most critical dimensions in the design, whereas the inlet and outlet lengths are not as relevant, above a minimum value.

With the purpose of understanding the effect of the critical design parameters on the effectiveness of the SPFR, we will carry out a simplified parametric analysis on reactor geometry, at different operative conditions (inlet flow rate and temperature, and reaction rate). The goal is identifying disguising effects due to poor surface contacting efficiency.

The sizing of the flow sections was selected to be consistent with the mechanical feasibility, assuming stainless steel as the reactor material. Also, dimensions were selected to minimize the gas residence time after the active surface, preventing secondary reactions in the gas phase. The only solid domain that was considered is the reactor base, below the active disk, for its relevance in heat conduction, assuming inert and impervious walls all around the flow region.

3.1. Governing equations

Within the fluid domain the following conservation equations hold:

1. Stationary, compressible total mass and momentum conservation (Navier-Stokes):

$$\begin{aligned} &\nabla \cdot (\varrho \boldsymbol{u}) = 0 \\ &\varrho(\boldsymbol{u} \cdot \nabla)\boldsymbol{u} = \nabla \cdot [-p\boldsymbol{I} + \mu(\nabla \boldsymbol{u} + (\nabla \boldsymbol{u}^T) - 2/3\mu(\nabla \cdot \mu)\boldsymbol{I}] \end{aligned} \tag{1}$$

These provide the velocity, $\boldsymbol{u}$ and the pressure, P distribution, in laminar flow.

2. Stationary, species conservation equations

$$\varrho(\boldsymbol{u} \cdot \nabla)Y_i = \nabla \cdot [\varrho D_i \nabla Y_i + \varrho D_i^T \nabla T/T] \qquad i = 1 \ldots NC \tag{2}$$

Eqs. do not account for any reaction in the gas phase, assuming that the heterogeneous reactions at the active surface prevail. Surface reactions appear as source (or sink) for the i-th species, at the catalyst's boundary. Solution of these equations provides the spatial distribution of the NC species mass fractions $\boldsymbol{Y}$.

3. Stationary, energy conservation equation

$$\varrho C_p(\boldsymbol{u}\cdot\nabla)T = \nabla\cdot(\lambda\nabla T) \tag{3}$$

Similar to Eq. (2), there is no generation or absorption of heat within the gas phase. It may occur at the boundaries, depending on their configuration (reacting, conducting, or adiabatic). The energy equation provides the T distribution within the gas domain.

Being the reactants usually very diluted, inert carrier properties were assumed for the gas phase. The entire set of Eqs. (1)–(3) are solved by the *CFD* simulation code, using state of the art numerical techniques [34].

3.2. Kinetics

With the purpose of parametrically studying the interaction of the active surface with the flow in the SPFR configuration, we simplified the heterogeneous reactions on the surface, assuming they can be described by a single, irreversible, bimolecular reaction among molecular species in the form:

$$\mathrm{A} + \mathrm{B} \rightarrow \text{products} \tag{4}$$

with the empirical rate law:

$$R'' = k^o \exp(-E_a/RT) C_A^{\alpha} C_B^{\beta} \tag{5}$$

providing the rate of surface reaction per unit surface, R'' as a function of the temperature and reactants concentration at the surface. Such a simplified chemistry (single reaction) will not allow speculating on selectivity effects, but it will be enough to highlight original and significant reaction-flow-temperature interactions.

3.3. Boundary conditions

Boundary conditions are classified according to the pertinent equations:

1. Compressible Navier-Stokes equations.
   Each internal solid surface is assumed to behave like a wall at rest, i.e. $\mathbf{u} = 0$. The normal velocity is determined at the beginning of the inlet channel, depending on the assigned flow rate. Zero relative pressure and zero viscous stress were set at the reactor outlet.
2. Stationary, species conservation equations.
   On each internal solid surface, except for the active surface, a zero normal flux of each species was imposed. The composition was set at the inlet, and null normal gradients (i.e. purely convective flow) set at the outlet. On the active disk surface, exposed to reactants flow, a net flux was imposed. The inflow of A and B are calculated from its consumption, through R'', according to the stoichiometry.
3. Stationary, energy conservation equation.
   The inflowing mixture was given a fixed temperature, that could be determined by a preheating section. The boundary solid surfaces were simulated as isothermal or adiabatic, as representative of two extreme, ideal configurations. On the active surface a net generation of heat given by $-R''\Delta H_r$ was imposed. Preliminary analyses have also been carried out neglecting the reaction enthalpy. Its effect is discussed in a following separate section.

3.4. Analysis of the simulation results

The simulations were carried out on a mixed triangular-rectangular mesh, the latter being used at the solid boundaries. The maximum element size was set at d/200 as determined by a mesh sensitivity analysis, for a total of 15,000 elements, typically, for the flow domain shown in Fig. 2. Results are reported focusing on the region closer to the catalytic surface, where the interactions between surface reaction and transport processes are more significant. Simulations provide very detailed information about the flow structure, the pressure, temperature and composition distribution. Unfortunately, most of these predictions cannot be confirmed by similarly accurate measurements. Local measurements by microprobes were used with some success in open SPF configurations [36]. However, the easiest measurements are carried out at the outlet, of the gas phase average composition. Accordingly, the most effective and interesting information is the reagents' conversion. It can be calculated from the simulations as

$$X_i = 1 - N_i^{OUT}/N_i^{IN} \tag{6}$$

where N_i is the molar flow rate (mol/s) of i-th reactant. While the inlet flow rate is known, the calculation of the outlet one is not obvious. It results from the integral of the normal molar flux, $\boldsymbol{n}_i^{\perp}$ (mol/s m^2), over the outlet section, S^{OUT}:

$$N_i = \int_{S^{OUT}} \boldsymbol{n}_i^{\perp} dS \tag{7}$$

4. Simulation and design of the novel SPF test cell

In the following, the results obtained by solving the SPFR model described above will be presented, as well as design indications formulated for its actual construction. We will first describe the common feature of the isothermal reacting flow (base case). Next, we will carry out a parametric study to investigate the role of the design parameters and their optimal combinations. Specifically, we will discuss the controlling processes inside the SPFR, including heat generation and transfer.

4.1. Base case

The detailed features of the results will be discussed on a reference set of conditions. We assumed that the reaction (4), bimolecular between molecular species A and B (thus thermal diffusion was neglected in Eq. (2)), occurs in a large excess of B. This may represent the common case of fuels (e.g. H_2, CO) oxidations, or gas sensing, carried out in excess of air. That allows simplifying the rate law to:

$$R'' = k^o \cdot \exp(-E_a/RT) C_A^{\alpha} \tag{8}$$

where the pre-exponential factor, k^o, will be assigned arbitrary values to compare fast or slow reactions. The activation energy determines the temperature effect on the reaction rate, so that realistic values must be given. We assumed a value of $E_a/R = 3300$ [K] based on an apparent activation energy for the reaction of H_2 with air on polycrystalline Pt [38]. The inlet concentration of key reactant A was assumed 1%mol. Other base case values are the inlet channel radius, $R_i = 1$ mm, the gap above the catalyst, $d = 1$ mm, unless otherwise specified, the inlet volumetric flow rate, $\dot{V}(298\ \mathrm{K}) = 100$ ml/min.

In the base case, the reactor was assumed isothermal, i.e. the reaction heat was neglected and the temperature assumed uniform throughout the whole reactor and flow domain, equal to the inlet temperature. The temperature was investigated within a range of 298–773 K. The effect of the reaction enthalpy is discussed in a separate section. Note that temperature influences both the reaction rate and the density of the mixture, affecting its velocity in the flow domain. The density of the mixture was determined assuming ideal gas behavior; its viscosity was assumed equal to N_2. The diffusion coefficient of A is assumed comparable to the mixture-average [24] value of H_2 in a 1% concentration in air. Further discussion on D_A will follow. All the transport and kinetic properties are temperature dependent.

With the reference set of parameters, the local velocity magnitude field is shown in Fig. S1 (Supplementary materials), in the stagnation point region. First, the effect of temperature on the velocity magnitude is evident. At higher temperature the reaction activates, locally affecting the flow, as shown in Fig. S1 (Supplementary materials) and better discussed below. A parabolic velocity profile easily stabilizes in the inlet channel, where laminar conditions always prevail. The inlet duct is the region with the highest velocity; laminar conditions here imply that the flow will be laminar everywhere else. Re numbers in the inlet vary depending on temperature and inlet diameter, but they are typically in the order tens, exceptionally reaching a few hundreds. The velocity magnitude drops dramatically when the flow diverges, in a geometry that expands the cross section by progressing from the center. This could be a concern for secondary homogeneous reactions that may evolve after the catalyst, at the higher temperature. It also suggests that the contact between the gas and the active surface lasts longer in the periphery of the disk. This is where most of the surface activity will be concentrated.

Fig. 3 shows the carrier streamlines at 298 K and 773 K. In both cases the laminar flow implies that most fluid never approaches the active surface. Reactants must diffuse across the stream, in order to reach the active surface. The diverging nature of the SPF configuration helps the process; when the radial velocity drops, the cross stream diffusion can compete with convection. The ratio between convective and diffusive flow appears to be crucial in understanding the interaction between reactive species and the active surface. This can be assessed through the A-species flux, in the flow domain, as shown in Fig. 4, which directly relates to the species consumption rate, at the surface. Still, Fig. 3 also shows a stagnation region near the corner, which is surprisingly larger at the lowest velocity (i.e. lowest temperature), whereas at higher temperature (lower viscosity), streamlines closely follow the corner. That is expected to impact on the supply of reactant A to the reactive surface (or viceversa, its possibility to bypass the surface by travelling farther from it).

The fate of the reactant *A* in the flow domain is well described by Fig. 4, where its total flux is represented by vectors. At the lower temperature (left panel) species *A* sticks to the convective field; reactant A reaches the surface almost entirely; it does not enter the wake beside the corner; the flux drops as the flow diverges; the surface uptake is very low, due to the low temperature that does not trigger the surface reactivity. At higher temperature (right panel), the sink of A on the surface is dominant and its flux after the active surface vanishes.

A more intuitive picture of the reactant A's fate is provided in Fig. 5, where its flow streamlines are indeed shown. It could be compared to Fig. 3, where the carrier streamlines are shown. Thanks to diffusion, the reactant can move across the convective flow to reach the surface. In turn, diffusion is driven by the rate of consumption of reactant on the surface. At lower temperature, only the molecules travelling very close to the surface can reach it. That occurs mostly in the peripheral region, where the convective velocity drops. Conversely, at higher temperature the surface is very reactive, causing a strong diffusive flux that can attract the reactant from the farthest regions. At the disk tip, diffusion can be even stronger than convection, causing species A to travel against the convective stream, in order to reach the active surface. The strength of the reaction has always to compete with convection, that keeps A flowing in the bulk of the gas, reducing its contact time with the catalyst and chances to diffuse across the main flow to reach the surface.

The previous Figures provide just a semiquantitative representation, and the actual impact on the overall A conversion between inlet and outlet must be evaluated, using Eqs. (6) and (7). This would be consistent with the experimental practice of surface activity measurements, were A conversion is determined by scanning of the temperature. In the simulations, we collect the results (in terms of X_A) of a sequence of steady state calculations, by varying the disk temperature (at isothermal conditions) or the inlet temperature (in adiabatic conditions). Eventually, all the results are shown as $X_A(T)$ curves. The results for the base case parameters, scanning the surface temperature from ambient to 773 K, are shown in Fig. 6. We can conclude that at the reference conditions, total conversion of *A* can be achieved above approximately 850 K. This value applies to a generic reaction $A + B$, with arbitrary kinetics. The actual value depends on the surface reaction rate which in turn is determined by the mechanism selected and the kinetics parameters. The values of the pre-exponential factor and activation energy are indicative. However, the absolute significance of the kinetics and involved parameters is not relevant at this stage, where relative comparisons are carried out.

The above discussion of the base case results gives interesting insight on the stagnation point flow reactor operation mode. The results suggest a thorough investigation of the effect of the parameters involved, and particularly those related to the geometry. The drop of the parabolic velocity profile, in the corner where flow diverges, and the abnormal velocity distribution, close to the catalyst surface, are a combination of transport mechanisms (convective and diffusive) and geometric features. The different streamlines configurations varying the temperature, close to catalyst surface, suggest a deeper investigation on the extent of diffusion limitation of the global process. Further, the precise identification of the geometric dimensions is a requirement for the subsequent realization of the laboratory reactor for testing disk-shaped active surfaces.

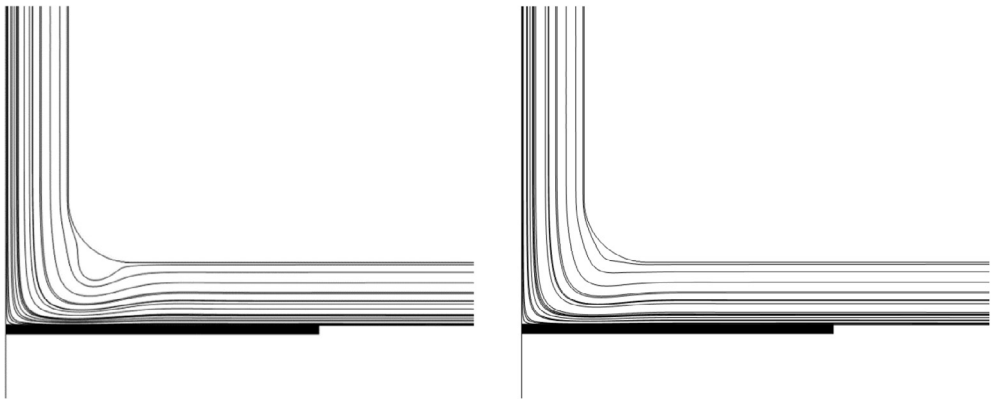

Fig. 3. Carrier streamlines in the flow domain. R_i = 1 mm, d = 1 mm, $k^o = 10^2$ m/s, $\dot{V}$ = 100 ml/min, T = 298 K (left), T = 773 K (right).

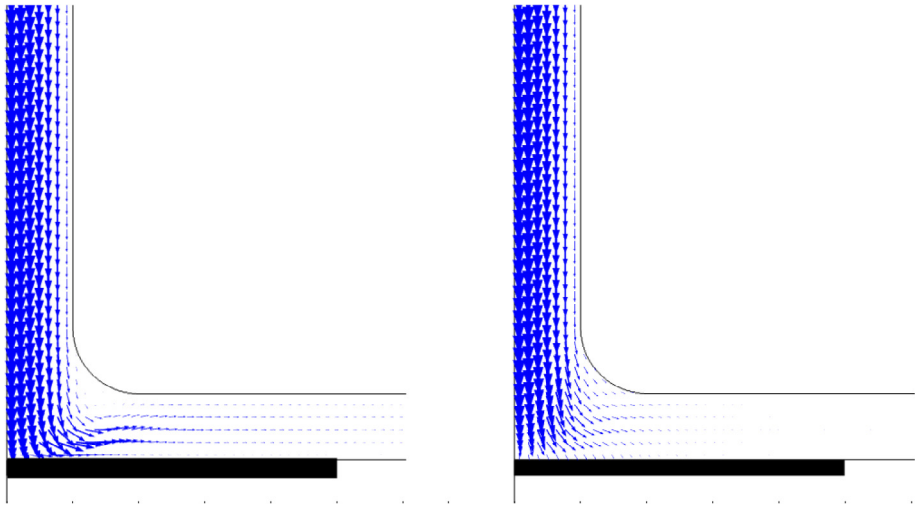

Fig. 4. Total (convective and diffusive) flow of reactant A close to the reactive surface. R_i = 1 mm, d = 1 mm, $k^o = 10^2$ m/s, $\dot{V}$ = 100 ml/min, T = 298 K (left), T = 773 K (right).

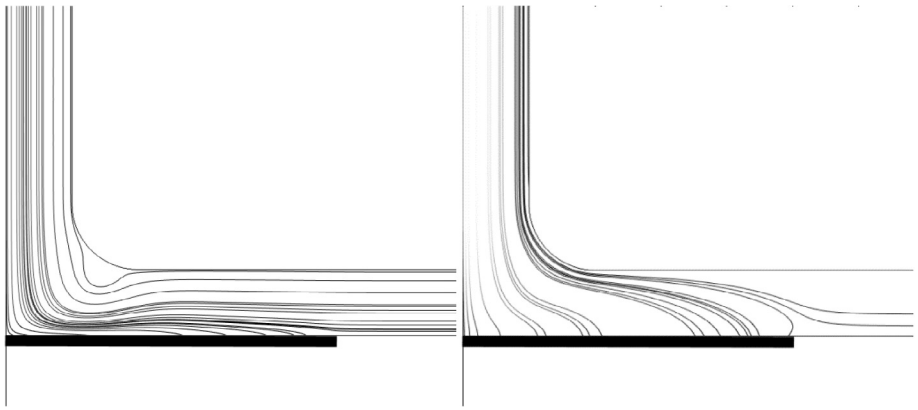

Fig. 5. Streamlines of A's flux close to the reactive surface. R_i = 1 mm, d = 1 mm, $k^o = 10^2$ m/s, $\dot{V}$ = 100 ml/min, T = 298 K (left), T = 773 K (right).

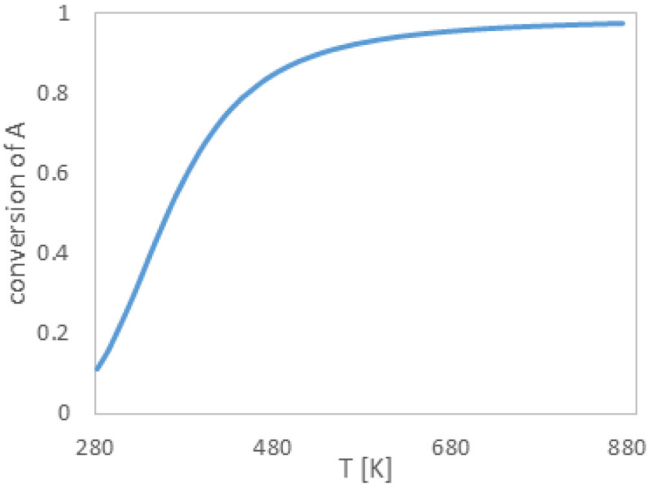

Fig. 6. Species A conversion across the whole test cell. R_i = 1 mm, d = 1 mm, $k^o = 10^2$ m/s, $\dot{V}$ = 100 ml/min.

4.2. Parametric studies

We evaluated several parameters effects; they are listed in Table 1, along with the space investigated. These are: the inlet total flow rate, $\dot{V}$, the radius of the inlet channel, R_i, the gap above the catalyst, (i.e. the height of the diverging section), d, the pre-exponential factor, k^o, and the surface temperature, T.

Table 1
Conditions and lengths for parametric analysis.

$\dot{V}$ [$mL_{STP}min$]	R_i [mm]	d [mm]	k^o [m/s]	T [K]
100 to 200	1 to 5	1 to 3	10^2 to 10^3	298 to 773

The range of temperature and flow rate are based on common experimental experience, including our own tests. The geometry is bound to effective stagnation flow, laminar regime, and mechanical feasibility, allowing for tolerances in the catalyst size and positioning.

4.2.1. Geometry

We simulated different widths of the inlet channel and of the gap above the catalyst, to identify the best dimensions for the final construction.

Fig. 7, left panel, shows that by enlarging the gap above the catalyst from 1 to 3 mm, the maximum conversion achievable decreases, as expected. A more active surface (higher k^o) can only achieve a higher conversion at lower temperature, but not at the highest, suggesting that a diffusion limited regime exists at the highest temperatures. Fig. 7, right, shows that the higher the total

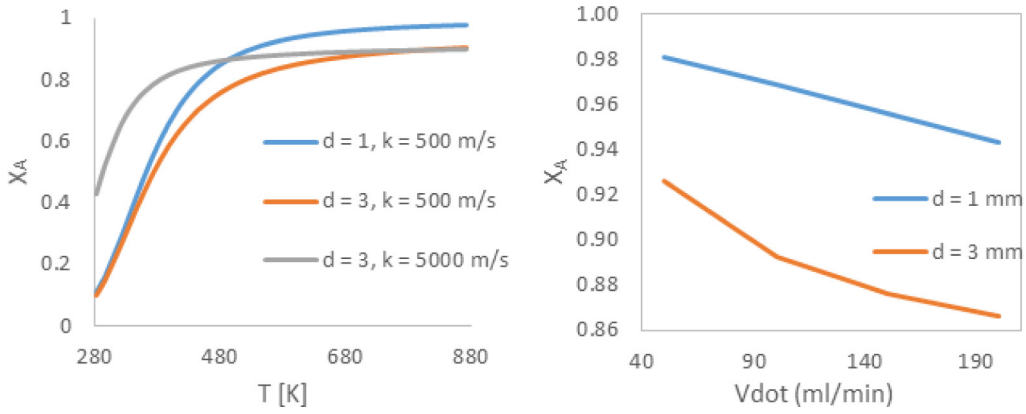

Fig. 7. Reactant conversion across the test cell as a function of temperature (left, $\dot{V}$ = 100 ml/min) and total flow rate (right, T = 773 K, $k^o = 10^2$ m/s) varying the gap d. R_i = 1 mm.

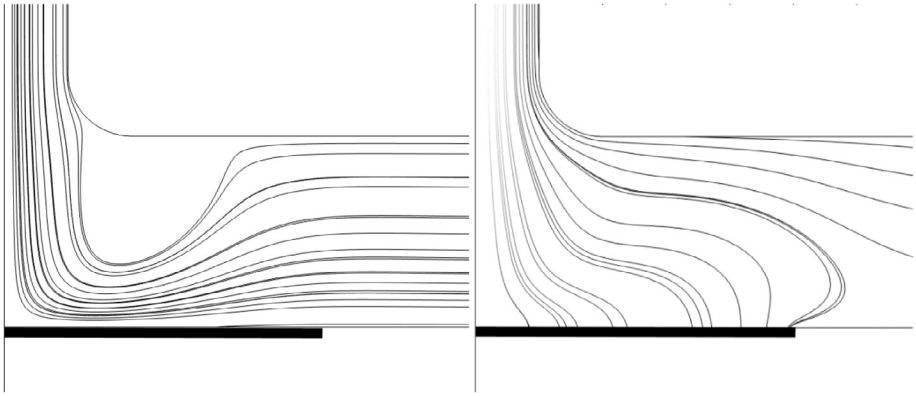

Fig. 8. Carrier (left) and species A (right) streamlines close to the active surface. R_i = 1 mm, d = 3 mm, $k^o = 10^2$ m/s, $\dot{V}$ = 100 ml/min, T = 773 K, d = 3 mm.

flow rate, the higher the effect of a larger gap above the surface, as a result of a modified contact time.

Increasing the gap above the catalyst, *d* also causes an enlargement of the region behind the corner where the velocity is very small, possibly with (irrelevant) backwards components, as clear from Fig. 8, left, compared to Fig. 5. In this region diffusion can easily dominate, bringing species A towards the active surface, where its concentration is lower, as shown in Fig. 8, right. Also, the dramatic increase of cross section determined by d = 3 mm causes such a drop in the local radial velocity that upstream diffusion occurs well beyond the disk tip (Fig. 8, right).

The interplay between convective and diffuse flux of species A is remarked in Fig. 9, where the two components were plotted with different colours. It is clear that diffusion prevails close to the active surface and especially at increasing radial distance. Consequently, by-pass of the active surface by reagents is clearly favored by larger gaps.

The effect of enlarging the inlet channel dimension, R_i, from 1 to 5 mm, on the reactant conversion is shown in Fig. 10. The maximum conversion decreases with a larger inlet channel. In the same Figure (left) we see that a more active surface (higher k) anticipates the reaction onset, but the incomplete conversion, due to diffusion limitations, remains. The different conversion due to the geometry is larger at higher flow rate, Fig. 10, right. An inlet channel as large as the active disk is expected to take advantage of the whole reactive surface, according to Fig. 11, right, where streamlines of A flux are shown. On the contrary, comparing with the case of R_i = 1 mm, Fig. 11, left, the reagent A reaches in both cases the catalytic surface, but the fraction that escapes without any contact is much larger using a wider inlet channel. The by-pass can be caused by the jet that is formed after the restriction, with a high local velocity, shown in Fig. S2. The jet prevails on the crossflow diffusion required to reach the active surface. We conclude that the larger inlet duct commonly used does not exploit the full potential of the active surface and is subject to severe diffusion limitation near the periphery of the disk.

The parametric studies at isothermal conditions allows us to conclude that the SPFR has to be built with the smallest possible diameter for the inlet channel and the minimum gap that can be reproducibly achieved above the active surface. Accordingly, given the mechanical tolerances and the approximation in the disk positioning in its seat, we concluded that the best configuration is R_i = 1 mm and d = 1 mm.

4.2.2. Contact time

It was observed that the flow and the reaction rates can affect the reactants' flow and consequently the final conversion of A. Keeping the optimal geometry identified above, we explore the parameter space of Table 1 for $\dot{V}$, T and k^o. In practice, the contact time of the gas with the active surface is investigated, and compared to its activity. Results are shown in Fig. 12.

Total conversion can always be approached if the reaction is fast enough and the flow rate is sufficiently limited, as shown in Fig. 12, left. Note that 200 ml/min is quite a high value for a test cell that has an inlet duct of 2 mm ID; the maximum velocity at 473 K approaches 4 m/s. Interestingly, at high gas velocity (because of the flow rate or temperature), some diffusion limitation may play

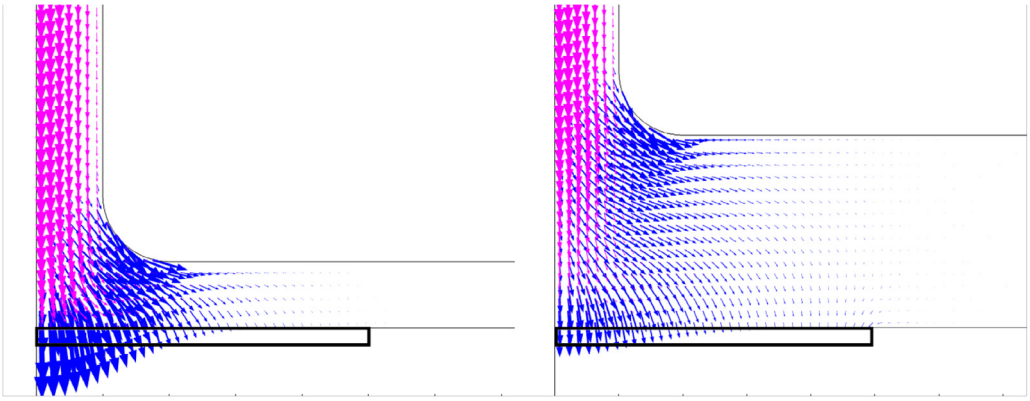

Fig. 9. Total (violet) and diffusive (blue) flow of reactant A close to the active surface. R_i = 1 mm, $k^o = 10^2$ m/s, $\dot{V}$ = 100 ml/min, T = 773 K, d = 1 mm (left) and d = 3 mm (right). Diffusive flux in the right panel is magnified ×10. (For interpretation of the references to colour in this figure legend, the reader is referred to the web version of this article.)

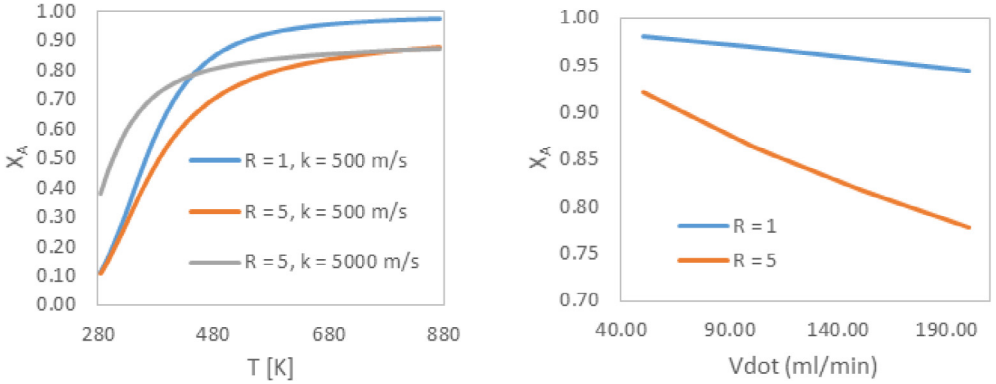

Fig. 10. Reactant conversion across the test cell as a function of temperature (left, $\dot{V}$ = 100 ml/min) and total flow rate (right, T = 773 K, $k^o = 10^2$ m/s) varying the inlet radius R. d = 1 mm.

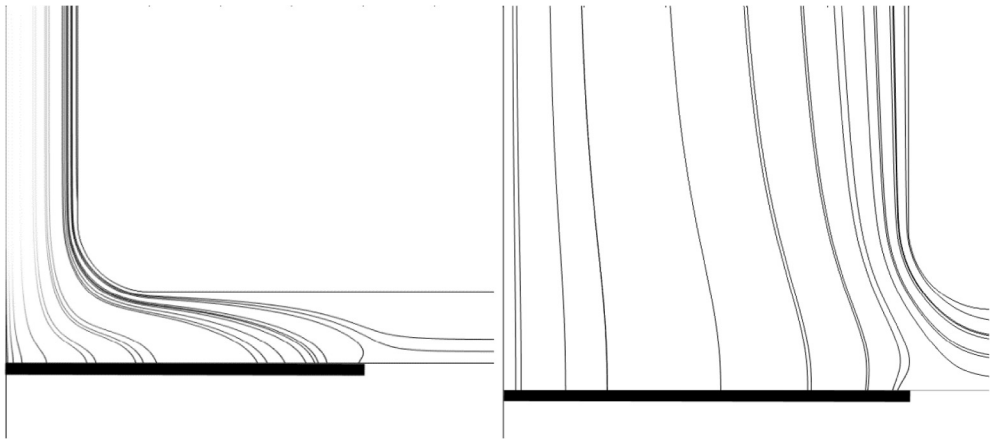

Fig. 11. Streamlines of A's flux close to the reactive surface. d = 1 mm, $k^o = 10^2$ m/s, $\dot{V}$ = 100 ml/min, T = 773 K, R_i = 1 mm (left) and R_i = 5 mm (right).

a role. The temperature appears less effective in advancing the conversion, as evident by the profiles being smoother, with a smaller positive derivative with respect to temperature. At a higher reaction rate, the conversion increases significantly also at quite high flow rate (small contact time), suggesting that the geometry identified is sufficiently free of diffusion limitations. We could formulate a criterion of equivalence in terms of a Damkhöler-type number k^o/u_{ref}, with a suitable reference velocity, but that would properly hold only for first-order kinetics and average properties [40]. Based on the results of thermal analysis presented later, we will not develop any further convection/diffusion criteria.

At larger total flow rate, the reagent contact time decreases, resulting in a lower conversion. This is confirmed by Fig. 12, right, at an intermediate temperature (473 K). The corresponding fluid velocity close to the active surface, slightly above it, along the radial direction, is shown in Fig. 13, as a function of the total flow fed. A lower flow rate obviously leads to lower velocity, meaning a longer contact time. The radial profiles always decrease, from the

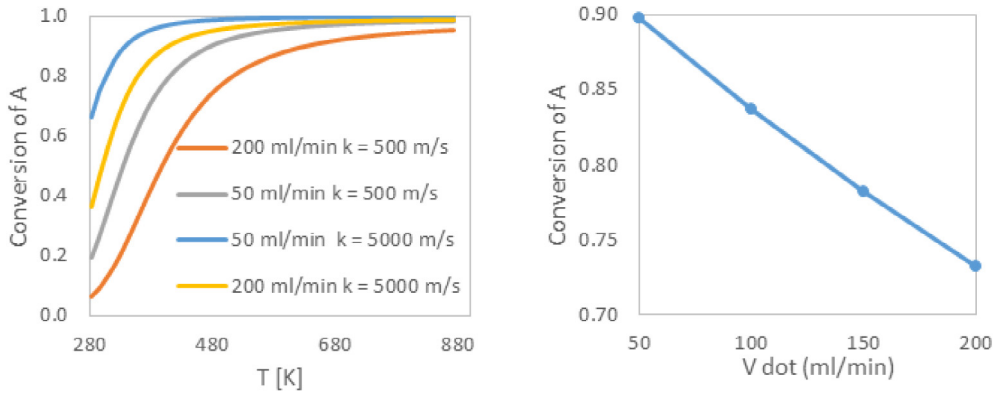

Fig. 12. Reactant conversion across the test cell varying the flow and the reaction rate, as a function of temperature (left) and total flow rate (right, T = 473 K, $k^o = 10^2$ m/s). R_i = 1 mm, d = 1 mm.

center to the periphery of the catalytic surface. This aspect suggests that reaction will be more effective on catalyst edges, and cross-flow diffusion will become dominant.

4.2.3. Diffusion rate

In order to double check the intuition that cross flow diffusion could be controlling, we varied the diffusion coefficient of A either by artificially reducing its value (using a scale factor) or including/excluding its temperature dependency.

We know that the diffusion coefficient of A in the inert carrier scales with temperature as

$$D_{A,inert} = \alpha D_{A,inert}(T^o)(T/T^o)^{\beta} \ [m^2/s] \quad (9)$$

where α and β vary for different species and mixture compositions, the latter being equal to 1.75 in Fuller's equation. The parameters in Eq. (9) were tuned on mixture-average values [24], calculated through the CHEMKIN code [38], using its property database. For a parametric study, α was reduced up to 5 times, to approach the ideal comparison of two different reagents A, such as H_2 and CO. The β values were changed from 0 to 1 (i.e. exclusion or inclusion of temperature dependence). The results are shown in Fig. 14. The first important observation is the large effect of the diffusion coefficient, which suggests that diffusive flux to the surface at high temperature can be a limiting factor. The second important indication is that the calculated conversion profile neglecting the effect of temperature on D_A (i.e. β = 0) shows a maximum, with lower values at the highest temperature.

This is not surprising, given that the higher temperature determines higher flow velocity and thus shorter contact time. The reaction rate also increases dramatically by rising the temperature; however, the conversion does not increase proportionally, as expected from a faster reaction, because of a limiting diffusion of reactants to the surface; that is amplified by the assumption β = 0 that implies that the diffusion coefficient cannot increase with temperature, where usually expected. In fact, in the high temperature region, the reaction rate is already very fast and the increase of conversion is actually controlled by the diffusion. The effect is magnified by the artificial reduction of the diffusion coefficient through the scale factor α = 1/5. The maximum at α = 0.2 can be considered the point of switch between the two controlling mechanisms. It must be recalled that the diffusion coefficient of H_2 is large compared with that of O_2, The diffusional limitations that are barely perceivable with a reactant A diffusing like H_2 are expected to be much larger with O_2 (or other reactants, such as CO). That can be relevant for reactions approaching stoichiometric (or sub-stoichiometric) O_2, in which O_2 diffusion can become the limiting factor.

The results of Fig. 14 clearly indicate that any kinetic study in this geometry, possibly with large reaction rates, requires an appropriate model of the fluid mechanics and mass transfer in the reactor flow domain, that can predict accurately the

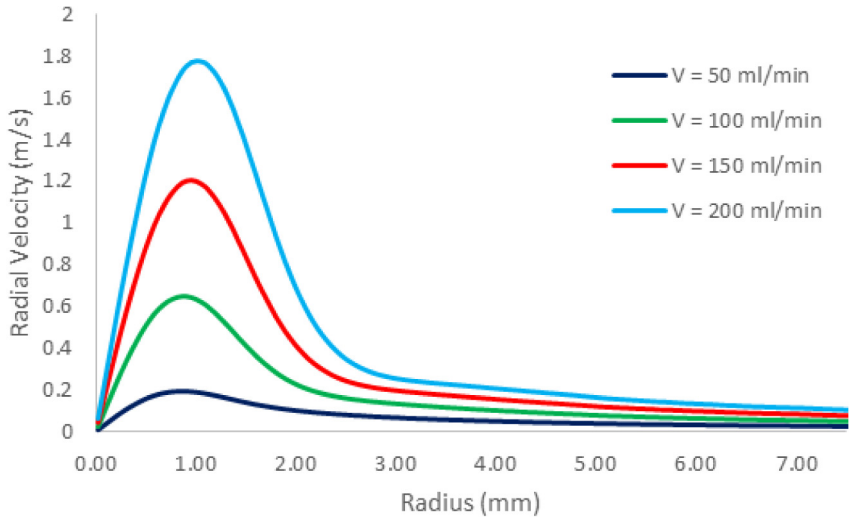

Fig. 13. Radial velocity profile slightly (d/20) above the catalyst surface, as a function of total flow inlet. R_i = 1 mm, d = 1 mm, $k^o = 10^2$ m/s, T = 473 K.

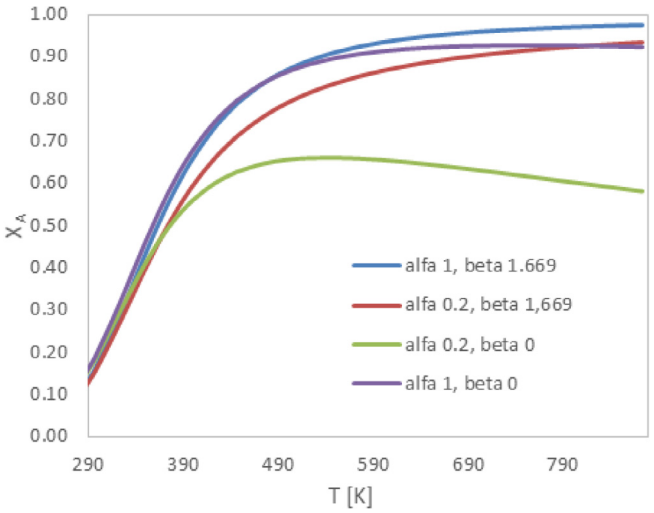

Fig. 14. Reactant conversion across the test cell as a function of temperature varying the reactant diffusion coefficient. R_i = 1 mm, d = 1 mm, $k^o = 10^2$ m/s, $\dot{V}$ = 100 ml/min.

interference (and limitations) that have to be ascribed to physical, not chemical, processes.

Limitations due to diffusional processes seem to be critical from the analysis above. However, all the calculations above do not consider the thermal effects of the reaction. Similar to the mass transfer limitations identified, also the heat transfer rate can play a role. Of course, that is not evident in isothermal flow simulations without the thermal effects of the reaction. However, as long as the Lewis number, $Le = \lambda/\varrho c_p D$, comparing heat conductions with mass diffusion, is close (or less) than unity for the limiting reagent, we can expect the reactions to be even more limited by the rate of heat conduction in proximity of the active surface. This aspect warrants a more detailed analysis, given that the temperature at the active surface heavily depends on the extent of the reactions and can in turn dramatically affect the surface reaction rate.

4.3. Thermal effects

The previous simulations neglected the heat of reaction, determining a uniform temperature in the whole flow domain. They provide some intuition on several features of the localized reaction, confined to the sample surface, depending on flow rate and its effect on the flow pattern close to the sample. The isothermal flow assumption is quite difficult to be approximated in practice, even if commonly assumed. More realistically, the uneven temperature distribution within the test cell, as determined by heat evolved (or absorbed) by the surface reactions, must be investigated. We expect significant modifications and consequences. The flow patterns in a gas, where density is extremely sensible to temperature, may change. The heat transfer properties of the mixture have to be taken in account. The temperature distribution will modify and the walls ability to transfer heat becomes crucial for stable and representative measurements.

4.3.1. Heat transfer model

The isothermal conditions simulated above were implemented by setting the whole reactor temperature (all solid surfaces, including the active surface), equal to the inlet mixture temperature. Still, the temperature effects were studied, properly adjusting the mixture properties that are temperature dependent, i.e. density, viscosity, and species diffusion coefficient. To include the thermal effect of the reaction in the simulation, the boundary condition at the reactive surface must be modified. The constant temperature condition on the active surface must be replaced by a given heat flux, locally varying according to the activity of the heterogeneous reaction. Considering a single, global surface reaction, its heat production flux from the surface is given by

$$q_0 = -R''\Delta H_r \qquad [W/m^2] \tag{10}$$

where ΔH_r is the reaction enthalpy. Exothermic reactions (i.e. $\Delta H_r < 0$) result in a positive q_0 consistent with a net heat release from the reactive surface. We assumed $\Delta H_r = -120$ MJ/kg, similar to the oxidation of H_2. The flux q_0 given by Eq. (10) entirely convected to the gas becomes the new boundary condition at the catalytic surface, replacing the isothermal condition applied so far.

The remaining surfaces of the test cell can be assumed either isothermal or adiabatic. These are two extreme behaviors of the metallic body. *Isothermal* surfaces assume that the cell's walls are able to match any inwards or outwards heat flux determined by the flowing mixture, including its heterogeneous reaction, to preserve a constant temperature. The *adiabatic* condition implies that the reactor's internal surfaces are totally unable to allow any heat flux, preserving the internal enthalpy. We simulated both scenarios, although none can be exactly reproduced in practice, due to technological limitations. Still, the actual behavior will be in between the two predictions. Note that additional properties, namely heat capacity and thermal conductivity of the gas mixture, become relevant.

4.3.2. Predicted thermal effects

Considering the reaction heat, we expect local temperature variations, which will affect the local velocity through the variable density. Representative calculations assuming either isothermal reactor walls (except the catalyst surface) and adiabatic conditions are shown in Fig. S3 (Supplementary materials) and Fig. 15. Results are reported for an intermediate inlet temperature (473 K). At this temperature the very different distribution that may occur, even at a weakly active surface, are more evident. Also, the pre-exponential factor was halved with respect to previous calculations, when the heat of reaction was neglected. Both facts (lower k^o and inlet temperature) reflect a much higher activity in the test cells, supported by the heat of reactions, that evolves in greater conversion at a lower inlet temperature. The higher activity may cause the calculations to fail in achieving convergence, reflecting dramatic gradients in the test cell, close to the reactive surface, hardly complying with the idealized boundary conditions. Concerns arise for larger inlet temperature. The consequent larger production of heat on the surface may cause dramatic hot spots in the

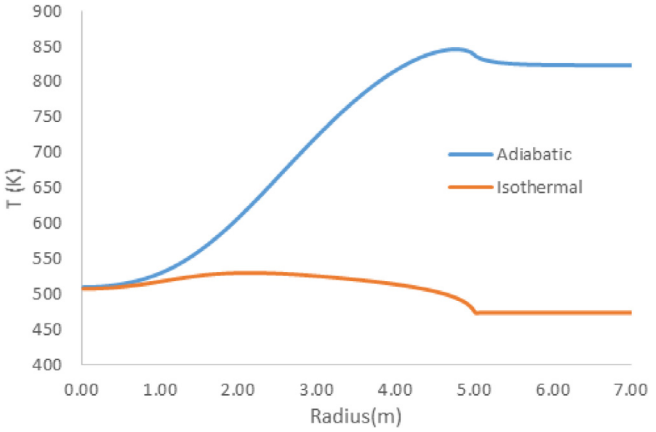

Fig. 15. Temperature of the gas at the bottom of the test cell, comparing isothermal and adiabatic reactor walls. k^o = 50 m/s, $\dot{V}$ = 50 ml/min, T_{in} = 473 K.

small flow gaps. It also suggests that experimental instabilities because of the reaction heat may occur.

Even with a moderate inlet temperature, the configurations shown in Fig. S3 result in an overall reactant conversion of 44% and 53% at isothermal (left) and adiabatic (right) conditions, respectively. The temperature rises significantly, beginning at the active surface where the exothermic reaction actually takes place, and more specifically at its periphery, where the contact time is larger Fig. 15. The maximum increase is approx. 60 K when keeping the non-reactive walls isothermal, but it can be as high as 230° in a fully adiabatic cell. Upstream of the active surface the temperature is not affected by the reaction heat, also at fairly low flow rate, in both cases. Note the small effect of the boundary condition (isothermal vs adiabatic) on the total conversion (+9%) compared with the huge difference (+170°) in the maximum temperature increase. However, the only relevant temperature is the one at the surface.

The clear indication is that the temperature distribution in the flow region can become very uneven, depending on the possibility to remove the reaction heat. However, even assuming an infinite heat removal rate (isothermal walls assumption), the temperature on the active surface will not be uniform. Thus, the 'catalyst temperature' can be an ambiguous concept, when experimental data are reported.

Temperature distribution combines with the different contact time between gas and active surface to result in a potentially very uneven local activity on the surface. The temperature along and near (0.5 μm) the active surface is shown in Fig. 16, in the isothermal wall assumption. The surface is colder close to the stagnation point (r = 0), because of the unreacted, cold gas impinging there. The divergence of the flow on the disk-shaped active surface implies a much smaller radial velocity at the periphery of the disk, as highlighted by Fig. S1 (Supplementary materials) and Fig. 13. A lower velocity causes a poor heat removal rate, a larger contact time, thus a greater reaction progress, ultimately causing a local temperature rise. The thermal wave is convected even more downstream, farther from the surface. The larger the flow rate, the larger the inner region of the disk which is isothermal with the inflowing mixture and the more peripheral the high temperature region. This is even more evident, also in Fig. S3, in the adiabatic case, were the reaction heat is brought to the bulk of the flow, well downstream of the disk.

Obviously, the regions at higher temperature on the active surface are more active, because of larger *k(T)*. Accordingly, the kinetic constant is larger in the peripheral regions; which may not correspond to a larger rate of reactant consumption, if its local concentration has already dropped due to the activity in the inner part of the disk, or just because of the diffusional limitations, in supplying enough reactant to the surface. The actual reactant consumption can be observed in Fig. S4, where the reagent diffusion rate is shown, comparing the previous simulation (neglect of reaction heat), with those allowing for the gas heating as a result of the reaction. Note that the diffusive flux at the surface is equal to the consumption rate per unit surface due to the reaction. The heat of reaction causes a higher surface temperature, then a larger rate of reactant consumption everywhere on the surface, Fig. S4, right, compared to the isothermal active surface assumption, Fig. S4, left. The activity on the surface spreads towards the disk tip, but does not achieve its maximum there, notwithstanding the higher temperature. As previously stated, this is a consequence of lower reactant concentration near the disk tip.

To verify the hypothesis that the periphery of the disk is not as active as expected because of limitations in the reagent diffusion from the bulk of the gas, we simulated a mixture where the reactant diffusion coefficient is larger. Now, instead of arbitrarily changing the diffusion coefficient with a multiplying parameter, as done in the previous parametric study, we changed the carrier properties. So far, it was assumed equal in properties to N_2 and the diffusion coefficient similar to the mixture-average value for H_2 in N_2. Assuming now that the carrier was He, the diffusion coefficient of a species like H_2 would be higher (approx. twice, at 473 K). The reagent conversion calculated for test cell using N_2 or He as carrier is shown in Fig. 17, as a function of feed temperature (left panel) and feed flow rate (right panel).

Unexpectedly, the reagent conversion is always higher in N_2 where its diffusion is slower. The shorter contact time (i.e. larger flow rates), Fig. 17 right, reduces the achievable conversion, as expected, but the N_2 allows larger conversion at any flow rate. It clearly suggests that reactant diffusion is not the controlling factor, unlike the results that neglect the heat of reaction.

Behind the apparent inconsistency of these results the effect of another important physical property must be considered, i.e. the thermal conductivity of the gas mixture. It is almost equal to the carrier property, given that reactant is assumed to be diluted (1%). The thermal conductivity depends on temperature, and at 473 K that of He is approx. 5 times the one of N_2. It determines the ability to remove the heat of reaction from the active surface. The temperature at and near the active surface using the two types of carriers are compared in Fig. 18, left. It is confirmed that the less heat conducting N_2 causes a much larger surface temperature,

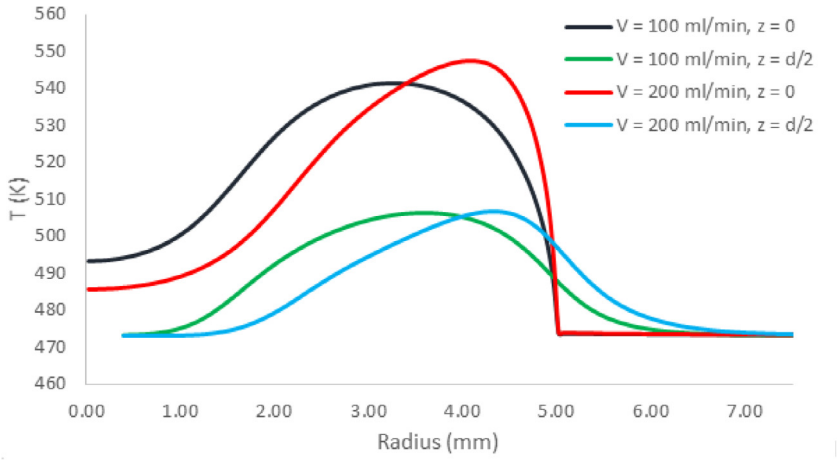

Fig. 16. Gas temperature distribution at and near (z = 0 and z = 0.5 mm) the active surface, along the radius. Isothermal walls assumption. k^o = 50 m/s, $\dot{V}$ = 100 and 200 ml/min, T_{in} = 473 K.

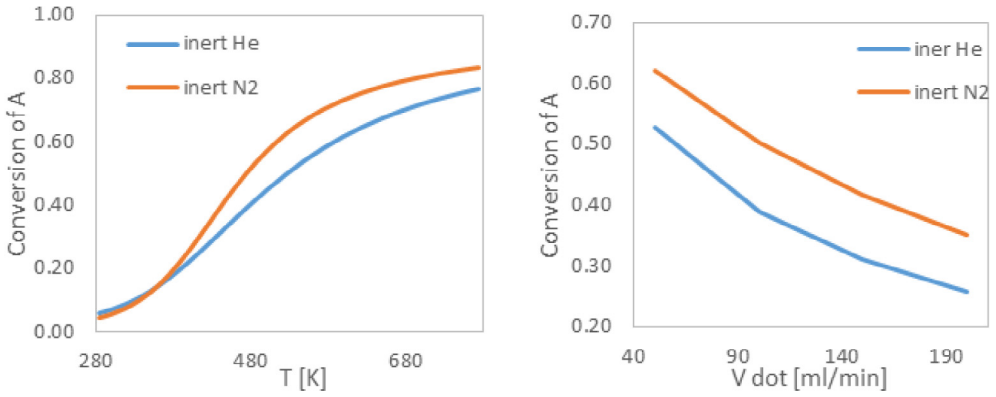

Fig. 17. Reactant conversion across the test cell feeding N_2 or He as carrier. Effect of inlet temperature (left, $\dot{V}$ = 100 ml/min) and total flow rate (right, T_{in} = 473 K), k^o = 50 m/s.

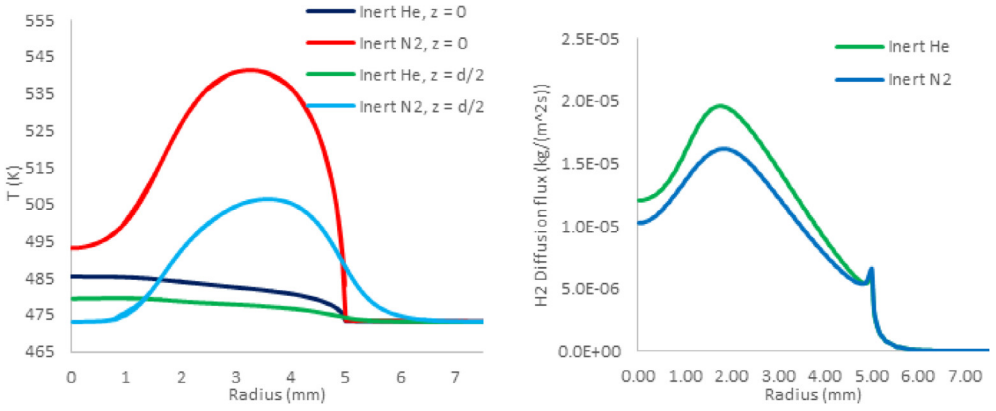

Fig. 18. Gas temperature distribution at and near (z = 0 and z = 0.5 mm) the active surface (left), and species A's flux at the surface (right), along the radius. N_2 vs He as carrier. Isothermal walls assumption. k^o = 50 m/s, $\dot{V}$ = 100 ml/min, T_{in} = 473 K.

resulting in significantly higher activity. Such a difference does not exactly reflect in a similar difference of consumption rate (that is equal to the diffusional flux of reagent to the surface, at steady state), as shown in Fig. 18, right, because the larger diffusion rate of reactant in He partly compensates in regions where the temperature with N_2 is higher. Still, the average consumption rate on the surface remains higher in N_2.

Summarizing, the analysis of the reaction heat effects shows that the reactive flow inside the stagnation point flow reactor is mostly affected by the localized heat generation on the active surface and the ability of the mixture and test cell to spread it rapidly and uniformly. Unless reactions with small ΔH_r are considered, very diluted mixture must be used to collect data at a reasonably constant surface temperature. Also, better heat conducting carriers (such as He) are preferred. The rate of diffusion of the reactants is less relevant, according to simulation based on a critical reactant having a diffusion rate comparable to H_2. The role of diffusion, which is controlling in isothermal conditions, can be more important for larger molecules as reactants (e.g. CO), whose diffusion rate is significantly lower than H_2.

We further verified the role of a realistic heat dissipation from the gas, including the heat conduction in the metal supporting the active disk. As already anticipated in Fig. 2, we added to the gas flow geometry simulated so far, the two solid domains, i.e. the active disk (assumed pure Pt) and the metal base (AISI 316 steel), extending 1 cm below the horizontal gas passage (see Fig. 2). Thermal properties of both Pt and AISI 316 steel were taken from Comsol Material Library. These will definitely conduct heat, affecting the gas temperature. We considered three boundary conditions at the periphery of the metal base: i) it has the same temperature of the inlet gas (i.e. the whole test cell is kept isothermal) ii) it is kept at 373 K (i.e. 100° below the inlet gas temperature) iii) it is adiabatic. Note that cases ii) and iii) are not duplicating the isothermal/adiabatic cases studied before. Now the metal base provides a path to distribute the heat generated at the active surface, reducing the local temperature gradients, verifying that the gas flow boundary is not perfectly isothermal or adiabatic, as in the previous calculation. The resulting temperature distribution near the active disk, including part of the metals domain (maps not reported), shows that the high conductivity of the metals causes negligible gradients in the solids. Still, the metal base supports a backwards heat transfer to the disk center, particularly in the adiabatic assumption, partially levelling the temperature along the active surface and neighboring region, as shown in Fig. 19.

Even if the difference might appear within a few degrees, the effect on the calculate reactant conversion across the whole test cell is significant, as shown in Fig. 20. Cooling the base (Tw < Tin) requires a larger inlet temperature to trigger the reaction onset, while the fully isolated base (adiabatic) causes the conversion to increase more rapidly, with the inlet temperature, until a point where the excess of heat production that cannot be remove leads to failure in convergence.

In summary, the numerical analysis above suggests building an actual SPF test cell with the smallest possible diameter for the inlet channel and minimum gap that can be reproducibly achieved above the catalyst. For example, the configuration R_i = 1 mm and d = 1 mm was deemed optimal for an appropriate reactive surface

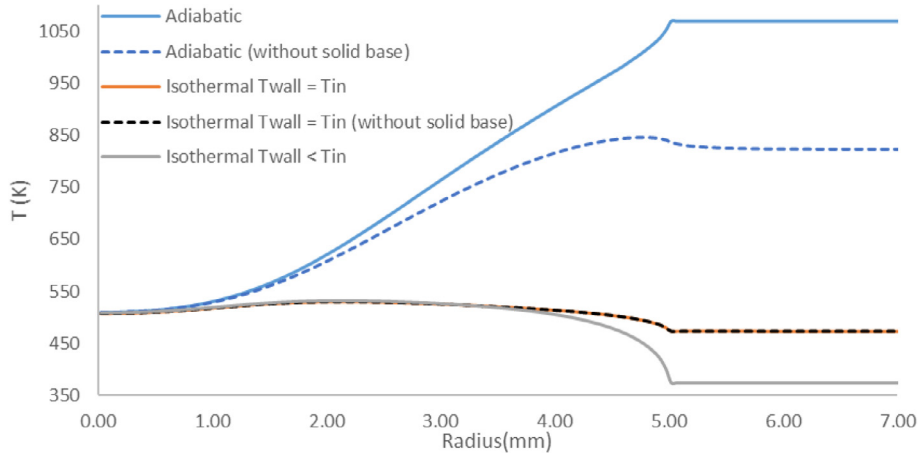

Fig. 19. Temperature distribution at the surface, near the active disk. Role of heat transfer in the metal base. k^o = 50 m/s, $\dot{V}$ = 100 ml/min, T_{in} = 473 K.

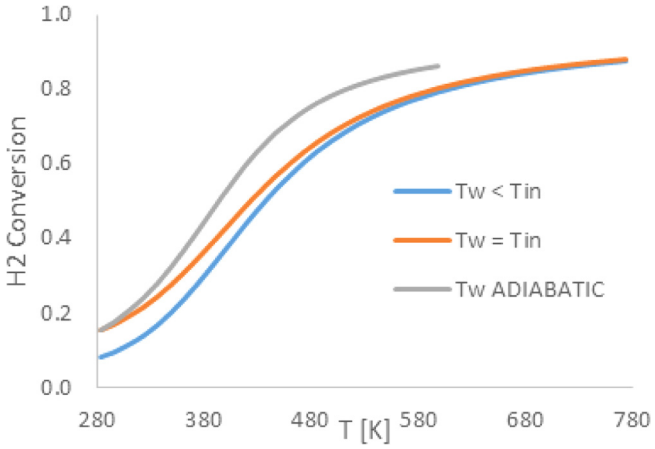

Fig. 20. Reactant A (similar to H_2) conversion across the test cell as a function of temperature. Comparison of different heat removal mechanisms. T_w is the temperature at the boundary of the metal base. k^o = 50 m/s, $\dot{V}$ = 100 ml/min, T_{in} = 473 K.

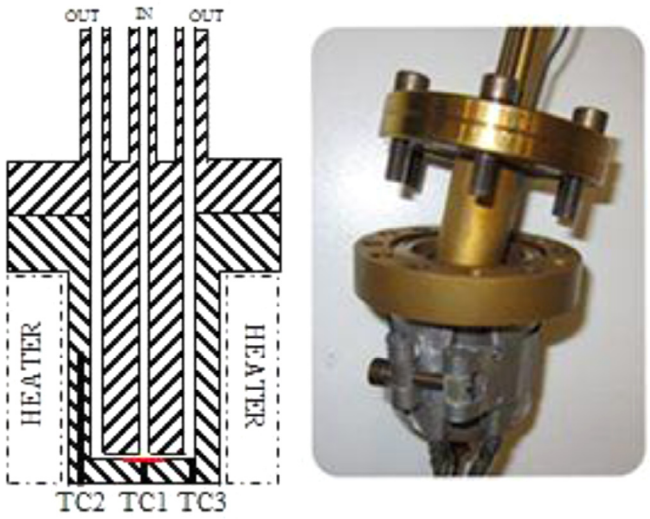

Fig. 21. Schematic representation (left) and a picture of the actual SPFR (right) as built, before thermal insulation is applied. The catalyst disk (red in left panel), is set on the bottom of internal part of the external body. (For interpretation of the references to colour in this figure legend, the reader is referred to the web version of this article.)

characterization. The thermal analysis suggests that the test cell body must be able to remove the reaction heat produced on the active surface, which in turn must be kept low either by using very diluted mixture or operating below full conversion. i.e. at lower temperature.

5. Experimental validation

On the basis of the previous parametric studies, an actual SPFR prototype was built. It was conceived to test disk shaped model surfaces, with a diameter and thickness of about 10 mm and 1 mm, respectively.

The easiest building strategy is made clear in Fig. 21. The reactor was obtained from two stainless steel bodies, identified by different colors in Fig. 21, left. They are coupled and hold together, as shown in the same Figure, right. The internal body has the inlet channel drilled at its center, pointing precisely to the center of the disk-shaped catalytic surface. Once paired, the two bodies allow for some space between them to collect the gas after the contact with the catalyst and bring it to the outlet pipes. The reacting mixture enters through the central channel, impinging orthogonally on the catalyst surface, then it flows radially from the center to the periphery of the internal body, escaping through the radial gap between the two parts and up to the two collecting pipes on the top.

The test cell shown in Fig. 21 keeps some design parameters adjustable while others had to be fixed. The gap above the catalyst can be modified using the appropriate spacers, between the two flanges where the two reactor parts are coupled. The total flow rate and the reactor temperature can be modified quite easily over sufficiently large ranges. Unfortunately, the inlet channel's radius cannot be easily modified. It was set to 1 mm. In principle, it can be modified as well, by inserting a liner in the channel that reduces its opening section. Finally, a titanium nitride coating was applied by chemical vapor deposition to prevent interactions between the reactants and the metals (e.g. Cr, Ni) and their oxides contained in the stainless steel of the reactor body. Reactor heating was provided by an electric band heater. It is regulated by a temperature controller (Omron E5CC). The set point is compared with the catalyst temperature, as measured by a thermocouple right below it. The entire reactor body and part of the piping was thermally insulated.

We tested the reactor using the H_2 oxidation on a Pt polycrystalline surface (SPL, The Netherland), acting as model surface. The focus is on trend comparisons, without claiming quantitative correspondance; no data fitting was done. Gas is fed through mass

flow controllers (Bronkhorst and Brooks) and mixed before entering the reactor. H_2 concentration in the feed is specified in the results, while O_2 is provided by synthetic air. N_2 was replaced by He in some tests, specified below. The outlet mixture composition was measured in parallel by a mass-spectrometer (HIDEN HPR-20 QIC, 0–200 amu), for high frequency, semi-quantitative analysis, and by a gas chromatographer (Agilent 7820), using a single MS5A packed column, 2 m long and TCD detection, using Ar as carrier; GC provides quantitative measurements at a lower sampling frequency·H_2O is not measured, due to the potential loss by condensation along the sampling lines. It was captured by condensation before gas analysis. The Pt surface was characterized by XRD, confirming its polycrystalline nature.

5.1. Temperature distribution

To verify the temperature distribution in the reactor body, because of the external heating and the internal flow of cold reagents, the reactor was equipped with 3 K-type thermocouples. Their actual positions are shown in Fig. 21, left panel. Because of the small thickness (1 mm) and the high thermal conductivity of platinum (71.6 W/m K at 300 K), the temperature measured by TC1, on the lower side of the Pt disk, was assumed representative of the upper side as well, the one directly exposed to the reactive mixture. The catalyst thermocouple is connected to the temperature control, whereas the other two were simply measured and recorded. We compared the measured temperatures in a nonreactive test, using an inert gas and inlet total flow rate $\dot{V}$ = 75 mL/min, with heating and cooling cycles. Results confirm that the assumption of isothermal reactor body, i.e. the temperature is the same in each part of it even during variable temperature measurements.

5.2. Conversion measurements

Simulations above provide useful indications concerning the optimal design parameters. They suggest semi-quantitative effects of the total flow rate, the catalyst temperature, the geometry and the transport properties (heat and mass diffusion rates). Here we aim at confirming its consistency with the experiments.

It must be recalled that the calculations assumed a simplified rate law, based on a single-step reaction that neglects adsorption/desorption steps and surface intermediates. Accordingly, the agreement between experiments and calculation must be qualitative, unless the catalytic process is effectively so simple in the kinetics, which is unlikely. Eventually, the SPFR will be used to develop and validate detailed surface chemistry models on different ideal surfaces. Here we simply aim at validating the SPFR as a reliable testing cell for kinetic studies, highlighting pros and cons. We investigated the stationary behavior of the reactor, i.e. at constant temperature. By measuring the outlet gas composition, we calculated the H_2 conversion to directly compare with the simulation indications.

For the catalytic hydrogen oxidation over Pt a reactive gas mixture of 7% H_2 in synthetic air is used. This is larger than 1% used in the simulation, to compensate for uncontrolled heat dissipation in the reactor, that smooths the carrier conductivity differences. The mixture is fed to the SPRF, and therein to the catalyst, starting from a cold reactor (room temperature). No H_2 conversion is measured at RT. The reactor temperature is gradually increased (2°/min) to a fixed value (443 K in this case). H_2 conversion is measured until a stable value is achieved. Fig. 22 shows the experimental results, at variable total flow, and spacers. It is consistent with the model predictions shown in Fig. 7, as expected. The flow rate affects both the catalyst contact time by the reactive mixture, the ratio of convective to diffusive reagents flow, and the temperature

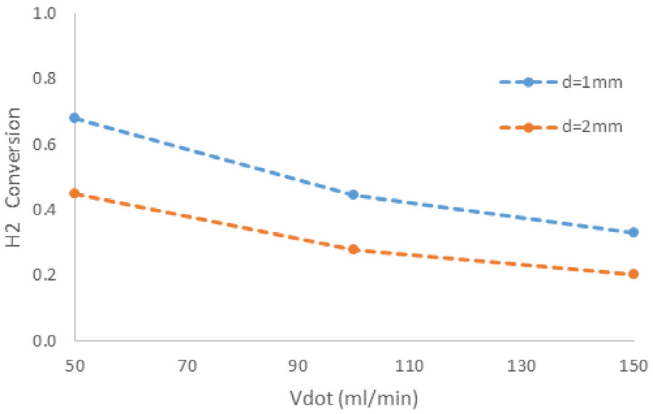

Fig. 22. H_2 conversion in oxidative tests on Pt, varying the total flow and the gap above the catalyst. Steady state measurements at 443 K. d = 1 and 2 mm, 7% H_2 in air.

distribution. Apparently, the influence on contact time and possibly on the heat exchange rate dominates. As a result, the H_2 conversion at fixed temperature decreases at larger flow rate, validating the predictions. Geometrical effects predicted by the model were validated using spacers to increase the gap above the catalyst, *d*. The experimental results are also shown in Fig. 22 where two configurations, with *d* = 1 mm and *d* = 2 mm, were compared, varying the total reactive flow. Note that the gap above the catalyst modifies the diffusive length for the reactants, that have to diffuse across the flow to reach the catalyst. Accordingly, the conversion is expected to decrease at a larger *d*, at the same total flow rate, as predicted by the model, see Fig. 7, and the measurements reported in Fig. 22 confirm these predictions.

Parametric studies also suggested a role of the diffusion coefficient of reactants in the reaction mixture. To validate the predicted effect we arranged the experiments with the same reactants but different inert gas. The goal is using an inert where H_2 diffusion is markedly different compared with nitrogen. If He replaces N_2, the mixture-average diffusion coefficient of H_2 at the inlet composition is about 1.6 times larger. The experimental results are shown in Fig. 23. They indicate that H_2 oxidation over Pt, using nitrogen as inert, leads to markedly higher stationary conversion values, compared to the cases using He as inert. Thus a higher diffusivity does not lead to a larger conversion. The effect of contact time (i.e. flow rate), remains as expected. The results confirm the simulation indications of the crucial thermal control. The diffusivity can control the conversion at conditions of high reactivity (high temperature)

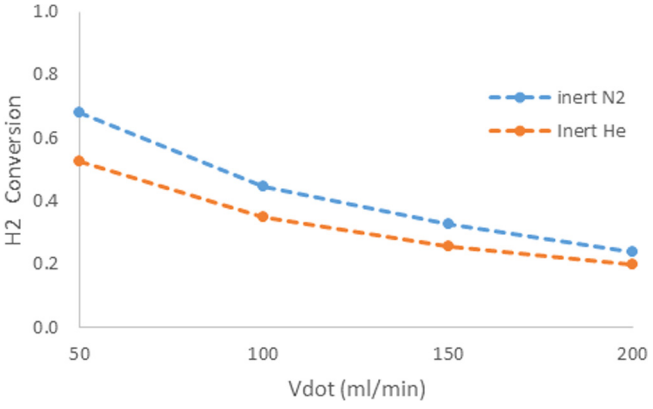

Fig. 23. H_2 conversion in oxidative tests on Pt, varying the total reactive flow and the carrier. Steady state measurements at 443 K. d = 1 mm. 7% H_2 in air or the equivalent O_2/He mixture.

only neglecting the thermal effects of the surface reactions. In practice, switching to He causes a significant increase of thermal conductivity, in addition to a larger H_2 diffusivity. According to the simulations, using He as carrier gas, the local temperature on the catalyst surface remains lower, being the conductive heat removal more efficient. Naturally, a colder surface leads to a lower conversion. The latter results confirm that the most crucial aspect of the SPF reactor is the local temperature distribution. To our knowledge, the possibility that a different inert gas could explain differences in measured light-off temperatures reported in the Literature, on the same reacting mixture has never been suggested, nor verified. Comparable effects of the carrier gas between experiments and predictions required a larger concentration of reactant in the experiments. In addition to larger heat dispersion in the actual reactor, compared to the predictions, the discrepancy suggests that in practice the heat transfer in the SFR is more effective than predicted by a laminar flow. A reason could be the onset of internal intrinsic oscillations in the flow [39].

6. Conclusions

We developed a small, versatile testing cell to experimentally study the activity of model surfaces, expected to be active for specific reactions. The ambition is to collect global reactivity data, as a result of the whole surface, to critically develop and analyze detailed surface kinetics, while keeping a non-local approach. The cell was conceived as a modification of the well-known stagnation-point flow arrangement, to operate under flowing gas, possibly at high pressure. We developed a mathematical model of flow, mass and thermal energy transport to investigate the potential and the critical factors affecting the cell's experimental indications. Through this model we carried out a systematic study of the constructive and operating parameters, using a model reaction (irreversible, first order). Specifically, geometric dimensions, contact time, temperature, rate of reaction, reactant diffusivity and heat of reaction were investigated.

Simulations indicate the crucial role of the reactor geometry in determining the effective contact between the reacting mixture and the active surface. Quite easily a large part of the mixture bypass the surface, resulting in a small overall conversion. At perfectly isothermal condition, if the flow passages are too large (3 mm is enough) the reaction can become diffusion controlled, by increasing the temperature. The diffusion path across the unmixed laminar streamlines can easily become excessive for reactants to reach the catalytic surface. The reaction heat dramatically affects the conversion achievable, becoming the controlling factor. A bottleneck was identified in the ability of the cell and the carrier to rapidly distribute and remove the reaction heat. The overall conversion in the stagnation reactor is much more affected by the thermal conductivity of the mixture than the reactants' diffusion rate, contrary to the expectation.

Finally, a prototype was built according to the indications of the parametric study, approaching a boundary layer, diverging flow from a centered feed orthogonal to a flat, model surface. The reactor is extremely simple its mechanical concept and versatile. It was operated using H_2 oxidation on a polycrystalline Pt disk as a probe reaction. Measurements confirm the consistency of the simulation study, revealing the unexpected critical role played by the local temperature distribution in the active surface region. Uncontrollable heat dissipations damper the predicted effects of the heat of reaction, experimentally observable at higher reactant concentration (thus larger reaction heat). Still, the local temperature in the experiments with stagnation flow is identified as the major source of uncertainty in validating microkinetic mechanism on model surfaces.

Acknowledgments

This study has been partially supported by the European Union's 7th Framework Programme under grant agreement no 280890-NEXT-GEN-CAT and H2020 Programme under grant agreement 686086-PARTIAL-PGMs.

Appendix A. Supplementary data

Supplementary data associated with this article can be found, in the online version, at http://dx.doi.org/10.1016/j.cej.2017.01.028.

References

[1] H.J. Freund, Model studies in heterogeneous catalysis, Chem.-Eur. J. 16 (2010) 9384–9397.
[2] M.S. Chen, D.W. Goodman, Structure-activity relationships in supported Au catalysts, Catal. Today 111 (2006) 22–33.
[3] L. Vattuone, L. Savio, M. Rocca, Bridging the structure gap: chemistry of nanostructured surfaces at well-defined defects, Surf. Sci. Rep. 63 (3) (2008) 101–168.
[4] J. Bandlow, P. Kaghazchi, T. Jacob, C. Papp, B. Tränkenschuh, R. Streber, et al., Oxidation of stepped Pt(111) studied by x-ray photoelectron spectroscopy and density functional theory, Phys. Rev. B. 83 (2011) 174107.
[5] A. Riemann, S. Fölsch, K.H. Rieder, Epitaxial growth of alkali halides on stepped metal surfaces, Phys. Rev. B – Condens. Matter Mater. Phys. 72 (12) (2005), art. no. 125423.
[6] J.V. Lauritsen, F. Besenbacher, Model catalyst surfaces investigated by scanning tunneling microscopy, in: Bruce C. Gates, Helmut Knzinger (Eds.), Advances in Catalysis, vol. 50, Academic Press, 2006, pp. 97–147.
[7] A. Ziegler, H. Graafsma, X.F. Zhang, J.W.M. Frenken (Eds.), In-Situ Materials Characterization: Across Spatial and Temporal Scales, Springer, Berlin, 2014.
[8] J.V. Lauritsen, F. Besenbacher, Model catalyst surfaces investigated by scanning tunneling microscopy, Adv. Catal. 50 (2006) 97–147.
[9] N. López, N. Almora-Barrios, G. Carchini, P. Błoński, L. Bellarosa, R. García-Muelas, G. Novell-Leruth, M. García-Mota, State-of-the-art and challenges in theoretical simulations of heterogeneous catalysis at the microscopic level, Catal. Sci. Technol. 2 (12) (2012) 2405–2417.
[10] M. Ehrensperger, J. Wintterlin, In situ scanning tunneling microscopy of the poisoning of a Co(0001) Fischer-Tropsch model catalyst by sulfur, J. Catal. 329 (2015) 49–56.
[11] M.P. Humbert, A.L. Stottlemyer, C.A. Menning, J.G. Chen, Bridging the materials gap between single crystal and supported catalysts using polycrystalline Ni/Pt bimetallic surfaces for cyclohexene hydrogenation, J. Catal. 280 (1) (2011) 96–103.
[12] D. Vogel, C. Spiel, Y. Suchorski, A. Urich, R. Schlögl, G. Rupprechter, Mapping the local reaction kinetics by PEEM: CO oxidation on individual (100)-type grains of Pt foil, Surf. Sci. 605 (2011) 1999–2005.
[13] R. Schlögl, Heterogeneous catalysis, Angew. Chem. Int. Ed. 54 (11) (2015) 3465–3520.
[14] M.K. Sabbe, M. Reyniers, K. Reuter, First-principles microkinetic approaches to heterogeneous catalysis, Catal. Sci. Technol. 2 (2012) 2010–2024.
[15] I.A.W. Filot, R.J.P. Broos, J.P.M. Van Rijn, G.J.H.A. Van Heugten, R.A. Van Santen, E.J.M. Hensen, First-principles-based microkinetic simulations of synthesis gas conversion on a stepped rhodium surface, ACS Catal. 5 (9) (2015) 5453–5467.
[16] A.B. Mhadeshwar, D.G. Vlachos, Hierarchical, multiscale surface reaction mechanism development: CO and H2 oxidation, water-gas shift, and preferential oxidation of CO on Rh, J. Catal. 234 (2005) 48–63.
[17] H. Ikeda, J. Sato, F.A. Williams, Surface kinetics for catalytic combustion of hydrogen-air mixtures on platinum at atmospheric pressure in stagnation flows, Surf. Sci. 326 (1-2) (1995) 11–26.
[18] G. Veser, M. Ziauddin, L.D. Schmidt, Ignition in alkane oxidation on noble-metal catalysts, Catal. Today (1-4) (1999) 219–228.
[19] Y.F. Zeng, R. Imbihl, Structure sensitivity of ammonia oxidation over platinum, J. Catal. 261 (2) (2009) 129–136.
[20] M. Rinnemo, D. Kulginov, S. Johansson, K.L. Wong, V.P. Zhdanov, B. Kasemo, Catalytic ignition in the CO-O2 reaction on platinum: experiment and simulations, Surf. Sci. 376 (1-3) (1997) 297–309.
[21] V.P. Zhdanov, Kinetic model of the hydrogen-oxygen reaction on platinum: istability, chemical waves and oscillations, Surf. Sci. 296 (2) (1993) 261–273.
[22] M.E. Garske, M.P. Harold, Observed kinetics of an exothermic reaction on a temperature-controlled catalytic wire, Chem. Eng. Sci. 47 (3) (1992) 623–644.
[23] X. Song, W.R. Williams, L.D. Schmidt, R. Aris, Bifurcation behavior in homogeneous-heterogeneous combustion: II. Computations for stagnation-point flow, Combust. Flame 84 (3-4) (1991) 292–311.
[24] R.J. Kee, M.E. Coltrin, P. Glaborg, Chemically Reacting Flow, Theory and Practice, Wiley, Hoboken, USA, 2003.
[25] M.E. Coltrin, R.J. Kee, G.H. Evans, E. Meeks, F.M. Rupley, J.F. Grcar, SPIN (Version 3.83): A FORTRAN Program for Modeling One-Dimensional Rotating-disk/Stagnation-flow Chemical Vapor Deposition Reactors, Sandia National Laboratories, 1991.

[26] D.G. Goodwin, H.K. Moffat, R.L. Speth, Cantera: An Object-oriented Software Toolkit for Chemical Kinetics, Thermodynamics, and Transport Processes, 2014, <http://www.cantera.org>.
[27] S. Matera, K. Reuter, When atomic-scale resolution is not enough: spatial effects on in situ model catalyst studies, J. Catal. 295 (2012) 261–268.
[28] C. Wang, S. Groves, S. Palmateer, D. Weyburne, R. Brown, Flow visualization studies for optimization of OMVPE reactor design, J. Cryst. Growth 77 (1986) 136–143.
[29] A. Mathews, J. Peterson, Flow visualizations and transient temperature measurements in an axisymmetric impinging jet rapid thermal chemical vapor deposition reactor, J. Heat Transfer 124 (2002) 564–570.
[30] B. Mitrovic, A. Gurary, L. Kadinski, On the flow stability in vertical rotating disc MOCVD reactors under a wide range of process parameters, J. Cryst. Growth 287 (2006) 656–663.
[31] N.E. McGuire, N.P. Sullivan, O. Deutschmann, H. Zhu, R.J. Kee, Dry reforming of methane in a stagnation-flow reactor using Rh supported on strontium-substituted hexaaluminate, Appl. Catal. A 394 (1-2) (2011) 257–265.
[32] S. Matera, K. Reuter, Transport limitations and bistability for in situ CO oxidation at RuO 2 (110): First-principles based multiscale modeling, Phys. Rev. B – Condens. Matter Mater. Phys. 82 (8) (2010) 085446.
[33] H. Karadeniz, C. Karakaya, S. Tischer, O. Deutschmann, Mass transfer effects in stagnation flows on a porous catalyst: water-gas-shift reaction over Rh/Al2O3, Zeitschrift fur Physikalische Chemie 229 (5) (2015) 709–737.
[34] <www.comsol.com>.
[35] D. Dalle Nogare, P. Canu, Plug flow vs. CFD modeling of CH4 partial oxidation on Pt in honeycomb, in: Proc. of CAMURE 8, Turku (Finland) May 22–25, 2011.
[36] S. Matera, M. Maestri, A. Cuoci, K. Reuter, Predictive-quality surface reaction chemistry in real reactor models: integrating first-principles kinetic monte carlo simulations into computational fluid dynamics, ACS Catal. 4 (11) (2014) 4081–4092.
[37] O. Deutschmann, S. Tischer, C. Correa, D. Chatterjee, S. Kleditzsch, V.M. Janardhanan, N. Mladenov, H.D. Minh, H. Karadeniz, M. Hettel, DETCHEM Software package, 2.5 ed., www.detchem.com, Karlsruhe, 2014.
[38] R.J. Kee, F.M. Rupley, J.A. Miller, M.E. Coltrin, J.F. Grcar, E. Meeks, H.K. Moffat, A. E. Lutz, G. DixonLewis, M.D. Smooke, J. Warnatz, G.H. Evans, R.S. Larson, R.E. Mitchell, L.R. Petzold, W.C. Reynolds, M. Caracotsios, W.E. Stewart, P. Glarborg, C. Wang, O. Adigun, CHEMKIN Collection, Reaction Design Inc, San Diego, CA, 2000.
[39] S. Mochizuki, Wen-Jei Yang, Self-sustained radial oscillating flows between parallel disks, J. Fluid Mech. 154 (1985) 377–397.
[40] M.E. Coltrin, R.J. Kee, Unified Nusselt- and Sherwood-number correlations in axisymmetric finite-gap stagnation and rotating-disk flows, Int. J. Heat Mass Transf. 102 (2016) 122–132.